Load path effect on the response of slender lightly-reinforced square RC columns under biaxial bending

Andrea Lucchini[a], José Miranda Melo[b], António Arêde[b], Humberto Varum[b], Paolo Franchin[a,*], Tiziana Rossetto[c]

[a] Department of Structural and Geotechnical Engineering, University of Rome La Sapienza, Rome, Italy

[b] CONSTRUCT-LESE, Faculty of Engineering (FEUP), University of Porto, Porto, Portugal

[c] Dept. of Civil, Environmental and Geomatic Engineering, EPICentre, Univ. College London, London, UK

* corresponding author paolo.franchin@uniroma1.it

Abstract

This paper presents an experimental investigation of the effect of load path on force-displacement response, damage patterns and failure modes of slender lightly-reinforced concrete columns. A review of available experimental tests that include columns subjected to multi-axial loading protocols is first presented. Next, a new experimental campaign on 18 column specimens tested under constant axial load and lateral displacement-controlled load paths is described. The results of the tests performed confirm that the response under biaxial load paths is qualitatively and quantitatively different from that observed for uniaxial load paths. The first and foremost qualitative difference is that the damage mechanisms change and the failure mode can change as a result. This, in turn, leads to the quantitative differences in ultimate and collapse deformation, and therefore ductility and hysteretic dissipation capacity.

Keywords

Failure mode; Damage pattern; Shear; Drift limits.

Introduction

Earthquakes impose multi-axial deformations on structural members, and especially columns. Despite this, current approaches to the displacement-based assessment of existing structures adopt deformation thresholds for performance limits that are based on uniaxial cyclic tests performed according to a single standard protocol (Elwood and Moehle 2005; Panagiotakos and Fardis 2001). For columns, verification is typically performed independently in the two orthogonal planes of deformation. So-called brittle failure modes are also checked independently in the two orthogonal planes, with a number of different shear strength models having been used for this check in the literature, e.g.(Priestley, Verma, and Xiao 1994; Kowalsky and Priestley 2000; Biskinis, Fardis, and Roupakias 2004; Sezen and Moehle 2004; Elwood and Moehle 2005). However, these shear strength models are also developed based on limited experimental data, which mainly comprise well reinforced columns tested using the same standardized uniaxial loading protocol and with only limited account of biaxial deformation. It is clear that such tests do not appropriately represent the range of response of columns with different detailing under earthquake loading. More broadly, observations of biaxial or triaxial (including variable axial force) response of RC columns are scarce, as summarized, e.g., in (Rodrigues, Varum, et al. 2013). In particular, there is a lack of such tests on structural members with inadequate transverse reinforcement. To the best knowledge of the authors, tests under multi-axial loading on columns characterized by low transverse reinforcement ratios (i.e., with $\rho_{sw} = A_{st}/bs < 0.15\%$, where b is the width of column section, A_{st} and s the area and spacing of transverse reinforcement, respectively) have been carried out only in (Boys, Bull, and Pampanin 2008) and Rodrigues et al. (2010; 2015a; 2015b; 2016).

As displacement-based assessment becomes the mainstream, there is an important need to develop multi-axial deformation capacity models. To do this, supporting experimental data needs to be created to highlight the qualitative and quantitative aspects of multi-axial response (Elwood and Moehle 2005). This paper first presents a review of available experimental tests that include columns subjected to multi-axial loading protocols. It then presents the results of a new experimental campaign on 18 column specimens tested under constant axial load and lateral displacement-controlled load paths (hereafter simply denoted as load paths). The purpose of this campaign is to investigate the effect of load path on force-displacement response, damage patterns and failure modes of lightly-reinforced columns. Finally, the results of the experiments are discussed, with qualitative and quantitative observations made as to the differences in column responses under the adopted load paths.

Review of previous biaxial and triaxial tests on RC columns

A survey of the literature on experimental tests was carried out to investigate biaxial and triaxial behavior of RC columns, and is summarized in **Table 1**, where the studies are presented in chronological order. Tests on specimens with reinforcement layouts and cross-sections typical of RC bridge piers are intentionally disregarded. Within this review, biaxial and triaxial tests denote, respectively, tests of columns subjected to biaxial bending and to combined variable axial load and biaxial bending. The table reports the shape of test specimen cross-sections along with data commonly related to the prediction of their failure mode, i.e. the axial force and aspect ratios, ν and L_V/h, the longitudinal and transverse reinforcement ratios, ρ_s and ρ_{sw}, the type of reinforcement bars and the presence of lap-splices. Response and failure mode are classified with the common tripartite distinction of flexural, ductile-shear failure (flexural yielding followed by shear), and brittle-shear.

Even though tests on RC columns subjected to multiaxial loading have been performed for more than three decades, only 83 individual biaxial and triaxial tests on RC columns were found in the published literature. Of these, 19 tests were actually found to be uniaxial tests that were conducted along non principal directions of the cross section (i.e. Joh and Shibata 1984; Ichinose 1996; Qiu et al. 2002; Rodrigues et al. 2015a). Hence, only 64 truly biaxial tests (reported in **Table 1**) can be said to exist; a number of tests which is orders of magnitude less than the amount of uniaxial cyclic tests published in the literature, e.g., (Perus et al. 2014). Further examination of the reviewed tests highlights that only 13 consider triaxial response (i.e. Li, Aoyama, and Otani 1988; Bousias et al. 1995; Rodrigues, Furtado, and Arêde 2016). Moreover, only one recent study is found that investigated the effect of load rate, i.e. the difference in biaxial response for static and dynamic application of the load orbits (Wang, Li, and Li 2013). As noted in Rodrigues et al. (2010), the scarcity of biaxial and particularly triaxial tests can be attributed to the higher complexity of the test setup (actuators, rig and monitoring system) required and the lack of standard multi-axial load paths.

Most of the reviewed experimental testing campaigns focus on square or rectangular column cross-sections, the only exceptions being two circular specimens in (Osorio, Bairán, and Marí 2012). Only one paper, (Boys, Bull, and Pampanin 2008), investigated the effect of lap-splices at the column base. Finally, all tests are on column specimens reinforced with deformed bars, with there being a total absence of tests on the biaxial response of RC columns with smooth bars. The only exception is represented by the plain R10 bar used for stirrups in the tests by (Boys, Bull, and Pampanin 2008), where longitudinal reinforcement is nonetheless deformed.

Several observations can be made on the response of RC columns under biaxial and triaxial loading from the reviewed tests:

- enhanced degradation in stiffness and strength under biaxial loading as compared to uniaxial loading: This is reported by all authors. It is also expected, since strength and stiffness are proportional in RC members, and it is well known that flexural strength is reduced by concurrent engagement in the orthogonal direction from simple interaction domain analysis;
- reduced ductility under biaxial cyclic loading as compared to uniaxial cyclic loading: This observation is consistent across all presented tests;
- unclear effect of loading on the energy dissipation capacity of the tested members: Some authors report an increase in energy dissipation due to biaxial deformation (Bousias et al. 1995), while others affirm the opposite (Qiu et al. 2002);
- significant increase in drift capacity associated with reduced axial load (Boys 2009; Elwood and Moehle 2005);
- angle between the vectors of the biaxial lateral displacement and the biaxial transversal load, namely, phase lag between the displacement and the load path;
- failure mechanisms observed under biaxial loading, are not necessarily predicted by uniaxial analysis of the element.

These findings will be compared with the response observations made for the test specimens in the new experimental campaign presented in this paper, which is specifically designed to investigate the effect of load path.

Specimens and experimental setup

Specimens

A total of 18 RC column specimens were tested in the experimental campaign. They were selected to represent, in general, columns of existing buildings designed according to old codes (such as for example those in force in Portugal until 1983, or as late as 1997[1] in Italy, prior to Min. LL. PP. 1997) with no stringent requirements in terms of detailing, and which allow lower area of shear reinforcement and larger stirrups spacing than would be acceptable in current building codes (for example, Eurocode 8). All columns have the same cross-section of 30x30cm and same the amount of longitudinal reinforcement, but are characterized by two different percentages of transverse reinforcement, denominated “low” (L) and “very low” (VL). Two values of applied axial load are used, equal to 150 and 450kN. In the test naming, these axial load values are represented by the numbers “10” and “20”, respectively, which refer to the corresponding approximate value of the axial load ratio (in percent). The two levels of axial load were established to represent inner frame columns at the third and the ground story of a four-story building (such as a typical low-rise building of the southern Europe region (Crowley and Pinho 2004)).

The geometry and reinforcement details of the specimens is presented in **Fig. 1**. The specimens represent half columns with 3.0m length (the lateral force is applied at 1.50m from the foundation top). Four continuous 16mm longitudinal reinforcing bars (deformed), which corresponds to a longitudinal reinforcement ratio of 0.89%, were adopted for all specimens. Stirrups of 6mm diameter were adopted for the transverse

[1] The very late date of introduction of mandatory seismic reinforcement detailing in Italy will strike the attention of any non-Italian reader, but it is also one contributor to the seismic vulnerability of the building stock. Interestingly enough, the prescriptions were more stringent pre-WWII and were relaxed in the following years.

reinforcement, spaced at 0.15m or 0.25m for the L or VL specimens, respectively. For all specimens, stirrups were anchored by 90° bends. The block foundation had 5 extra stirrups of 10mm diameter in each direction to prevent damage in the foundation during the tests. The concrete cover adopted for the columns and block foundation was 2.5cm and 2.0cm, respectively.

Table 2 reports for the four groups of columns, identified through the value of the transverse reinforcement ratio (ρ_{sw}) and the axial load (N), a summary of the mean material properties in terms of: concrete cylinder compressive strength on 2:1 samples with 15cm diameter (f_c), yield strength (f_y) and ultimate tensile strength (f_u) of the longitudinal reinforcement steel, yield strength (f_{yw}) and ultimate tensile strength (f_{uw}) of the transverse reinforcement steel.

Load path selection

Fig. 2 illustrates several uniaxial (a-c) and biaxial (d-m) testing protocols that have been used in past experimental campaigns. Protocol (a) consists of symmetric cycles repeated for a fixed or variable number of times at a given drift level before moving to the next, larger, drift level. This is the standard SAC protocol (Krawinkler et al. 2000) and can be considered representative of most cyclic tests carried out on structural components. Originally developed for the assessment of steel structures under the design-basis earthquake, it has been varied in terms of number and amplitude of cycles and used in several research studies also for materials other than steel, as well as for the investigation of the response of structural components at incipient collapse. In this latter case, however, symmetric cyclic loading may lead to excessive cumulative damage not representative of the actual seismic demand prior to collapse. This issue has been clearly highlighted in a number of studies (e.g., FEMA 2009, Krawinkler 2009) and recently discussed by Suzuki and Lignos (2020). Asymmetric loading protocols, such as the SAC near-fault loading history (Krawinkler et al. 2000) of **Fig. 2** (b) and the collapse-consistent loading protocol (Elkady and Lignos 2016) of **Fig. 2** (c), were also proposed to replicate, respectively, the effects of near-fault ground motions, and load paths of structures that experience cycles around accumulating permanent drifts in one direction while approaching collapse.

Recognition of the need to investigate multi-axial response of columns has led to the formulation of biaxial loading protocols, as shown in **Fig. 2** (d) to (m). Protocol (d) consists of alternating uniaxial cycles in the two orthogonal plan directions, and, although biaxial, it is not particularly realistic as an earthquake does not alternate loading direction in a systematic manner. Modified versions of this biaxial loading protocol are shown in (e) to (g), which have been used in many studies (**Table 1**). In these protocols, the displacement is applied simultaneously in the two orthogonal plan directions, but through paths which are characterized by straight segments that can not be considered as representative of the actual curved displacement orbits caused by earthquakes. (Boys, Bull, and Pampanin 2008) attempted to use a realistic loading protocol, shown in **Fig. 2** (h), in their biaxial column tests, however, they report that the irregularity of the loading protocol made the interpretation of the response measurements difficult. Therefore, they propose in the same paper protocol **Fig. 2** (j), a modified form of the cloverleaf protocol **Fig. 2** (i), which in turn is a rounded variant of protocol **Fig. 2** (g). Similar regularization of actual displacement orbits have been proposed by others, e.g. by Elkady and Lignos (2016). The latter work expands the idea of collapse-consistent protocols, proposing one in biaxial deformation, shown in **Fig. 2** (k).

In the experimental campaign reported in this paper a uniaxial monotonic (UM) and the traditional uniaxial cyclic symmetric (UCS) loading protocol of the type shown in **Fig. 2** (a), are used as reference cases, and to provide comparisons with other experiments in the literature. In addition, a uniaxial cyclic asymmetric protocol (UCA), similar to that in **Fig. 2** (c), is considered. Linear elastic analysis of simple systems under two-component motions carried out by the authors during the test design have shown both paths similar to those in **Fig. 2** (i) or (j), as well as others of more circular nature, like those in **Fig. 2** (l) or (m). However, the latter two biaxial protocols, here labelled Biaxial Circular (BC) and Biaxial Elliptical (BE), were chosen for the experimental campaign as they allow for an investigation of the effect of different proportions of maximum displacement amplitude in the secondary direction.

Table 3 summarizes the load paths adopted for all the 18 RC column specimens. It is noted that the total number of tests is not distributed evenly among the considered four groups of columns due to economic constraints limiting the number of test specimens. It was decided to conduct most tests on the specimens with very low transverse reinforcement with high and low axial load ratio, and with low transverse reinforcement with high axial load ratio, due to the relative scarcity of such tests in the literature. These specimens were the focus for comparison of RC column performance under varied load paths.

The axial load was kept constant during the tests. Cyclic lateral displacements were imposed, in the N-S direction only, for the uniaxial load path, and in both the N-S and the E-W direction, for the biaxial load paths. For the latter, the N-S is the direction along which the first increment of displacement is applied, as well as the main direction of loading for the BE tests. Three and two cycles were repeated for each lateral displacement level imposed for the columns tested under symmetric (UCS, BE, BC) and non-symmetric (UCA) load paths, respectively. The symmetric load path consists in the following ± nominal peak displacements in mm: 3; 5; 10; 4; 12.5; 15; 7; 22.5; 30; 37.5; 45; 52.5; 60; 67.5; 75; 82.5; and 90 (which, in the case of the tested columns, correspond to percentage drift ratios respectively equal to: 0.2; 0.33; 0.67; 0.27; 0.83; 1; 0.47; 1.5; 2; 2.5; 3; 3.5; 4; 4.5; 5; 5.5; and 6). The non-symmetric displacements path includes the following peak displacements in mm (drift ratio demands in percentage): +5, -5; +10, -10; +15, -15; +25, -10; +35, -5; +45, 0; +55, +5; +65, +10; +75, +15; +85, +20; and +95, +25 (+0.33, -0.33; +0.67, -0.67; +1, -1; +1.67, -0.67; +2.33, -0.33; +3, 0; +3.67, +0.33; +4.33, +0.67; +5, +1; +5.67, +1.33; and +6.33, +1.67). The biaxial tests only differ of the uniaxial ones because have two horizontal actuators instead of one. In the circular path, the amplitude of the peak displacement is the same in the two directions, while in the elliptical one is twice in the N-S than the E-W direction. The detailed histories of the lateral displacements imposed in all cyclic tests are shown in Appendix 1.

It is highlighted that most of the cycles are performed in the plastic range, since the yield displacement of all the specimens is around 10mm, as confirmed in the tests and approximately estimated before with the usual relations :

$$\phi_y = 1.75 \times \frac{\varepsilon_y}{h} = 1.75 \times \frac{0.002}{0.3} = 0.012m^{-1} \tag{1}$$

$$s_y = \frac{\phi_y L_V^2}{3} = \frac{0.012m^{-1}1.5^2m^2}{3} \cong 10\ mm \tag{2}$$

where ϕ_y is the curvature at yielding calculated according to Biskinis and Fardis (2010), ε_y is yield deformation of the reinforcement steel, h is the depth of the column cross-section, L_V is the shear length, and s_y is the yield displacement.

Experimental setup

The experimental setup is the same as that described in Rodrigues, Furtado, and Arêde (2016) and in (Rodrigues, Arêde, et al. 2013), except for the apparatus adopted to restrain the base of the specimen, which consists of a stiff steel socket anchored to the strong-floor of the laboratory. The specimen is assumed to act as a cantilever, where the inflection point of a 3.00m column height is located at its mid-height (H = 1.50m). **Fig. 5** represents the general view, the test setup schematics and the sliding device used to apply the axial load. The axial load and the two lateral loads are applied by three independent servo-actuators fixed on two steel reaction frames and a concrete reaction wall. As the axial load actuator remains in the same position during the test, a steel sliding device was developed to transfer the axial load to the column specimen. The sliding device is formed of two low friction sliding steel plates and is placed between the actuator and the top of the column (**Fig. 5** (c)). The friction force at the slider is derived, in each of the two orthogonal horizontal directions, from the equilibrium of the upper plate as the sum of the force measured by the "Friction load cell" (as denoted in **Fig. 5** (c)) and the lateral resisting force offered by the vertical actuator. Calibrations made by the authors in previous experimental campaigns showed that this latter contribution can be estimated by multiplying by 2.2 the lateral displacement of the vertical actuator, with the force and the displacement being expressed in kN and mm, respectively.

When the column deflects laterally, a (small) moment is actually applied at the top of the member by the vertical actuator. This is the consequence of a p-delta effect (which reduces to zero at the base), as well as of an uneven distribution of pressure which is applied by the vertical actuator to the column through the rotational hinge connected to the friction sliding steel plates. This moment, which is a function of the axial load level

(N), moves down the inflection point at a height from the base (H_i) that can be approximately estimated as follows:

$$H_i = (1 - y/100)H \tag{3}$$

$$y = -0.0137N + 17.348 \tag{4}$$

where N is expressed in kN, and Eq. (4) derives from authors' past calibration results obtained for the maximum displacement allowed by the testing machine.

Based on the above, and from basic equilibrium considerations, it follows that the moment at the base of the column can be obtained by multiplying the lateral resisting force of the member (which is derived from measurements as described in the next section) by the product between the nominal shear span length H and the correction factor $(1 - y/100)$, which in the case of the tested columns is equal to 0.85 and 0.89 for the lower and higher axial load level, respectively. The drift ratio, on the other hand, can be estimated as the lateral top displacement of the column divided by H, since the error caused by assuming the inflection point being located at a distance H from the base instead of H_i can be considered as negligible. In fact, it is easy to demonstrate that the error on the drift is smaller than that on the height of the inflection point, and in the case of the tested columns is in the order of 5%.

Instrumentation and measured responses

The force and displacement of each actuator was recorded with a load cell and an internal LVDT, respectively. The lateral displacement of the column in the directions of loading was measured at several heights, through wire position transducers attached on faces N and W, for the biaxial tests, and on face N only, for the uniaxial tests. At the horizontal actuator level, the lateral displacement was also measured by a LVDT attached to an external reference frame. One strain gauge was installed on each longitudinal reinforcing bar, 10cm above the top of the foundation. The deformation of the column faces was measured by recording the relative displacements of several points using LVDTs, most of which were located at the plastic hinge level. The layout of these sensors as well as those used to measure the horizontal forces and the absolute displacements are shown in **Fig. 6** and **Fig. 7**.

In post-processing the results, the actual lateral top displacement of the column and the corresponding resisting force were obtained. To do this, the (small) rotation of the foundation was measured in the two directions by a biaxial inclinometer, and the contribution to the lateral top displacement of the column was calculated and then subtracted from the horizontal displacement recorded by the sensors. The lateral resisting force of the column was obtained as the force measured in the horizontal actuator minus the corresponding friction force, obtained as described before, which reached maximum intensities in the order of 30% the maximum force applied by the actuator.

The relative displacements measured with the LVDTs attached to the face of the column were used as shown in **Fig. 8** to derive the shear and the flexural contribution to the lateral deformation of the member at the plastic hinge level. The face LVDTs measure the deformations of a frame whose bottom vertices (1 and 2) are connected rigidly to the base, while the top ones (5 and 6) are free to deform together with the column. Deformations between the vertices are measured vertically (D15 and D26), horizontally (D56) and diagonally (D25 and D16). As demonstrated in **Fig. 8**, the shear angular distortion γ, and therefore the corresponding contribution s_{shear} to the lateral deformation of the frame, can be obtained from the total rotation of the vertical side of the frame α, and the rotation caused by flexure only, which is equal to half the rotation of the top side of the frame θ. In turn, α and θ can be calculated using simple trigonometric relationships from the deformed lengths of the horizontal and vertical sides and the diagonals of the frame. Note that the shear displacement can be calculated four times, because measures from each of the two vertical sides of the frame can be used to derive the angles, and because measures from LVDTs attached to two parallel faces are available for each direction of interest (N-S or E-W, respectively). s_{shear} is therefore estimated as the mean of the four measured shear displacement values.

Test results

Failure modes and damage patterns

Failure modes of reinforced concrete members are usually classified into shear (also termed brittle shear, i.e. shear failure before flexural yielding), flexure-shear (also termed ductile shear, i.e. shear failure after flexural yielding) and flexural (Hua Jingjing et al. 2019), as well as splitting (Pham Thanh-Phuong and Li Bing 2014; Ichinose 1995), the latter being more rarely observed.

Unless documentation of the sequence of phenomena leading to failure is exhaustive, (e.g. by making the whole data set available numerically together with high-quality photographic material), researchers using data from other experimental campaigns have to rely on the attribution of failure mode given by the authors of the original research. For instance, compilers of the PEER Structural Performance Database (Berry, Parrish, and Eberhard 2004), used by several others to develop predictive equations of the failure mode, classify columns as follows: based on (1) shear damage reported by the experimenter, (2) observed resistance (compared to the value calculated from a moment-curvature analysis), and (3) displacement ductility at failure. A column is flexure (F) critical if no shear damage was reported by the experimenter, otherwise it is shear (S) or flexure-shear (F-S) critical, depending on whether the response is brittle or moderately ductile, respectively. Note that, according to such a classification, a F-S critical member is strictly one for which the post-yield response is affected by shear.

Similarly to the PEER Database, this work also uses the term "failure" to denote beginning of significant degradation of the post-peak lateral resistance, but distinction is made between terms "shear-critical" and "shear-sensitive": the first one refers to the failure mode, and is reserved for columns failing in shear, which for the tests of this campaign occurred always after flexural yielding (i.e., for columns classified as F-S). The second term is used to denote a column whose deformation is significantly affected by shear, but which can then fail in flexure. Moreover, to provide readers with a more detailed description, "damage pattern" indicates the specific sequence of damage phenomena leading to a particular failure mode (which can be different for the same failure mode). "Collapse" is defined as the loss of axial load-bearing capacity (identified in the tests from the significant increase of the vertical downward displacement), which may occur after failure.

As illustrated for the sake of brevity with reference to the monotonic tests only by the plots of **Fig. 9**, all columns of this campaign are characterized by a shear-sensitive type of response. The horizontal axis reports the drift calculated at the point where the lateral load is applied, i.e., at a height of 1.50m from the base. The vertical axis reports in absolute (middle row) and relative (bottom row) terms the contribution of shear s_{shear}

in the plastic hinge zone (z = 400mm) to the total deformation s_{tot} of that zone, computed as shown earlier in **Fig. 8**. In the test VL20UM, yielding is identified from deformations of the tension-side longitudinal bars as measured by strain gauges. The corresponding drift is used to determine the yielding point also for test L20UM, since strain gauges' measurements in this case were not reliable. Also, in this latter test s_{tot} is not the record of the wire position transducer, which did not work properly, but derived from LVDTs measurements. Since strain gauges were not used in test VL10UM, in this case the reported value of drift at yielding is actually the one observed in the corresponding UCA test. The plots show that shear contribution is minor before flexural yielding, and significantly increases to account for half of the displacement after the yield point. It is apparent that the deformation of the columns is mainly caused by the flexural response, but that it is also “sensitive” to the shear contribution.

The failure mode in each test, which is reported in **Table 4**, was identified based on the observed damage. Failure in shear was attributed to columns that exhibited an inclined through crack along which sliding occurred, coupled with following loss of both horizontal and vertical load-bearing capacity of the member. For some tests, the failure mode was not clearly observed, thus the attribution is in brackets in the table. In the case of the test VL10UM, despite the presence of a large inclined crack, sliding and then collapse did not occur since the test stopped because the maximum displacement allowed by the testing machine was reached (≅100mm, i.e., 6.5% drift). In tests L20BE, VL20BE and VL20 BC, on the other hand, diffused shear cracking made it difficult to recognize sliding plane. It is interesting to note that all columns subjected to the higher level of axial load are characterized by a flexure-shear failure. Columns under the lower level of axial load, instead, are F or F-S critical, depending on the considered loading protocol, as shown by the classification of tests VL10. Such an influence of the load path on the failure mode was also observed by Umemura and Ichinose (2004), and confirmed, recently, by Opabola and Elwood (2021) in an experimental study on poorly detailed gravity columns under uniaxial cyclic loading.

For both failure modes F and F-S observed in the campaign, different damage patterns were identified. These are shown in **Fig. 10** and **Fig. 11** for the monotonic and the cyclic tests, respectively. Damage observed in the cyclic tests is illustrated through six columns selected as representative of groups of columns that exhibited a similar pattern. The figures show, in particular, the damage observed in the column at the maximum lateral force, at the beginning of the strength deterioration, and at the end of the test, and the response history of the column both in the horizontal and vertical direction. Regarding the latter, it is useful to note that the upward displacements are produced mainly by rotation of the top section (caused by flexure), and to a lesser extent, presumably in cyclic tests only, by elongation of the column (as the result of crack opening along the column height, as explained by Sezen 2020). The downward displacements, on the other hand, are produced by the rigid body motion of the top part of the column suddenly caused by shear failure and consequent sliding along a diagonal crack, or by shortening slowly caused by reduction of the cross-section area, mainly due to flexure. The upward displacement that follows the drop (recorded in the monotonic tests) are caused by removal of the applied axial load.

In the flexure critical columns, failure was caused by buckling of the longitudinal bars. Loss of lateral resistance was then reached due to rebar fracture (NC), or as a consequence of loss in vertical load-bearing capacity caused by significant concrete degradation (C). In the case of the flexure-shear critical columns, four damage patterns were observed: concentrated shear cracking, followed by collapse caused by sliding along a large diagonal crack, a) with contribution to shear resistance given by dowel action of the longitudinal bars and concrete, through aggregate interlock and shear resistance of the compressed zone (Rig_Sl_Cc), for VL cases when the crack does not intersect stirrups, or b) by dowel action, concrete and the stirrup (Rig_Sl_ St) in the L cases; c) shear cracking and formation of a larger inclined crack merging with a vertical crack located along one of the longitudinal bar, followed by collapse because of sliding, the latter being resisted by both concrete and the single stirrup that crosses the crack which finally opened or broke (Dmg_Sl_St); d) diffused shear cracking with larger inclined and vertical cracks similar to those previously described, followed by collapse with no clear sliding plane observed (Diff_Crk). A detailed description of the sequence of damage observed in the cyclic tests is given in the Appendix 2, and it is summarized here in the plots of **Fig. 12**, which report the values of the drift (in the main, N-S, direction of loading) recorded at the following damage states: beginning of flexural cracking, beginning of shear cracking, spalling of the concrete cover, failure (i.e., opening or fracture) of the stirrup (the one involved in the shear failure mechanism of the column), first buckling of the longitudinal bars and first fracture of the longitudinal bars.

Based on the observation of damage in all tests, the following comments can be made. In flexure-critical columns, loss of the vertical load-bearing capacity, when it occurs, is likely due to core concrete area reduction caused by increased concrete crushing induced by biaxial loading (compare damage patterns of tests UCS and BE-BC). In flexure-shear critical columns, biaxial cycling produces diffused cracks leading to a shear failure which may not exhibit a clear sliding plane (i.e. compare damage patterns of tests UM-UCA-UCS and BE-BC). Contribution of concrete to shear resistance within the truss tension mechanism is not negligible: in tests VL10UM and VL20UM no stirrup crosses the main diagonal crack along which sliding occurs. In L tests shear failure mainly involves the second stirrup from the base, with the contribution of the first one being negligible. Fracture of the stirrup (observed only in the test VL20UCS) may be caused by a hook bending at slightly more than 90°, which prevents the hook opening and forces the stirrup rupture in tension.

Effects of load path on response

The plots of **Fig. 13** show the results of test L20BC and can be considered as representative of the cyclic response observed in all the biaxial tests. These plots show how the column's response in the main direction of loading, i.e., the N-S direction, is modified because of imposed displacements in the orthogonal direction, i.e., the W-E direction. When the first increment of displacement is applied in the N-S direction, the displacement in the orthogonal W-E direction is zero. The maximum force is measured at the maximum displacement and is oriented near to the N-S direction (cyan circle marker).

When biaxial cycling starts, it causes plastic deformations in the W-E direction. In order to reach the maximum displacement in the N-S direction at zero deformation in the E-W one, a force has to be applied along E-W and this reduces the N-S force at peak N-S displacement (next circle markers). As a consequence, the peak force (within each cycle) occurs at a lower displacement amplitude than the maximum and the curves exhibit softening, which is related to damage due to orthogonal loading. This behavior is observed as phase lag between the displacement (i.e., the deformation) and the force path, as shown in the N-S vs W-E force plots. It is interesting to note that the phase lag changes during the loading history, being larger at imposed peak displacements in the W-E direction (than in the N-S direction), and increasing with the increase of ductility demand. The latter is clear if the results obtained for cycling at drift values ±1.5% are compared with those at

±2.1%. Also, the phase lag does not change within the sequence of cycles at constant drift. These observations denote the dependency of the phase lag on the level of plastic deformations and on the direction along which the first excursion into larger plastic deformation levels takes place.

As pointed out in (Rodrigues, Varum, et al. 2013), phase lag between the force and displacement vector under imposed biaxial deformation has been observed as early as in the mid-1970s (Takizawa and Aoyama 1976), with reference to square load paths, and later by (Saatcioglu and Ozcebe 1989) for elliptical and (Panagiotakos and Fardis 2001; M. N. Fardis and Biskinis 2003) for circular ones. It has been associated with higher energy dissipation, but, as explained above, it is associated with the additional damage induced by the orthogonal loading, not with a larger energy dissipation capacity (i.e. a given damage, associated with a given dissipated energy, is simply reached at an earlier drift in biaxial deformation).

Fig. 14 compares the monotonic responses with the envelopes of all cyclic tests. Because column L10 was not tested under monotonic loading, in the top left panel of the figure the response of the VL10UM test is reported as a reference curve. Also, in each panel the monotonic curve in the negative quadrant is the zero-point reflection of the curve in the positive quadrant, which is the actual measured response. It is recalled that for the biaxial tests, the N-S direction corresponds to the main direction of loading, i.e., the one along which the first increment of displacement amplitude is imposed, and in the case of tests BE (those with elliptical orbits) the direction corresponding to larger displacements. It is also highlighted that VL10BC is the test that, unlike the adopted BC protocol, ended with a final monotonic push after a significant reduction in the lateral strength was recorded.

By looking at the plots of **Fig. 14** it can be observed that at given drift demand, reduction of strength and increase in post-peak slope, caused by cyclic loading, increases from UCA, to UCS, BE, and BC, i.e., along with that of the level of dissipated energy through cycles. Larger strength degradation, as the effect of a lower transversal reinforcement (compare the corresponding curves in the top and bottom panels), is more pronounced in the case of higher axial load (i.e., for those columns failing in shear) and uniaxial load-path (i.e., in those tests corresponding to a lower cyclic degradation). As expected, an increase in the axial load increases the strength and reduces the ductility of the columns. Lastly, strength is slightly lower in the pull direction than in the push. This asymmetry is likely due to effects related to direction of first displacement increment, such as buckling which occurs first in the bars located on the pull face, as a consequence of previous larger plastic excursion in tension.

Fig. 15 illustrates, through the results of four tests, how the envelope of the force-drift in the N-S direction is used to determine the values of the ultimate drift ratio θ_u and the drift ratio at collapse (axial failure) θ_a. As shown in the top-left panel of the figure, θ_u is defined as the drift at the point of 20% strength loss. This is the widely used definition of the ultimate point by Park and -S. Ang (1985), which allows the obtained experimental values to be compared with those reported in many other research studies (e.g., Panagiotakos and Fardis 2001; M. N. Fardis and Biskinis 2003). θ_u can be considered as a proxy of the drift at the beginning of significant strength degradation, which is caused in a F critical column by buckling of the longitudinal bars (or significant concrete crushing) and in a F-S critical column by shear failure. The minimum absolute value of θ_u^+ and θ_u^- obtained from the response of the column in the positive and negative direction of loading (i.e., the push and pull direction, respectively), is considered as the value of the ultimate drift capacity θ_u. As reported in the bottom right panel of the figure, for the F-S critical columns where 20% drop of strength is not observed (because of premature collapse caused by in-cycle deterioration) θ_u is set equal to θ_a. This latter is defined as the maximum drift, and it is calculated only for those columns which are characterized by loss of the vertical load-bearing capacity (simply denoted as collapse in **Fig. 11**). In order to account for the push and pull direction of loading, θ_a is defined similarly to θ_u as the minimum of the absolute values recorded in the positive and negative direction (θ_a^+ and θ_a^-, respectively). Recall that loss of the vertical load-bearing capacity is caused by concrete crushing and consequent reduction of the resisting area of the cross-section for F columns. In the case of the F-S critical columns, loss of vertical load-bearing capacity is instead caused by the sliding of the upper portion of the column along a main diagonal shear crack. As the top-right panel of the figure reports, for some F-S critical columns the actual value of θ_a is not available because the maximum travel of the actuator did not allow for the point of complete loss of the vertical load-bearing capacity to be reached. These cases are denoted by a value of θ_a > 6.5%. It is important to highlight that while in a F-S critical column loss of the lateral load-bearing capacity is combined with loss of the vertical load-bearing capacity, in a F critical column loss of vertical load-bearing capacity is observed only in cases of cross-section reduction due to significant in-cycle deterioration (possibly due to biaxial loading, as in the case of the tested columns classified as F/C in **Table 4**).

The results reported in **Fig. 15**can be used to make two further observations. First, the maximum drift that a column can sustain, especially in the case of ductile F critical members, strongly depends on the load path. This is clearly shown by the bottom-left panel plot, which reports the results of the test VL10BC. This case shows that after a significant strength reduction caused by cycling loading, the column can still exhibit a significant residual deformation capacity if a further monotonic increment of displacements is imposed. This explains why the columns were seen to collapse under cyclic loading but not in the monotonic tests. This observation, which is consistent with findings of several past experimental studies, agrees with the assumption of the largely used damage index of Park and Ang (Park and -S. Ang 1985), according to which damage is a function of both the maximum deformation and the effect of repeated cyclic loading. The influence of the load path on the seismic capacity of the columns will be also illustrated in the later discussion on the values of θ_a obtained in all tests. It is important to highlight that evidence of such strong variability raises questions as to the value to consider for θ_a when collapse capacity of the structure is evaluated through a pushover analysis, or when a phenomenological model that does not explicitly describe in-cycle degradation is adopted for the hysteretic behavior of columns (see for example the model of Zhu L., Elwood K. J., and Haukaas T. 2007). Obviously, this issue becomes more critical for structures that are located in seismic areas that are affected by both ordinary and pulse-type ground motions, i.e. in the case of structures subjected to excitations which are significantly different in terms of number and amplitude of imposed cycles. Secondly, the bottom-right panel plot of **Fig. 15** shows that collapse, as also observed by other researchers (e.g., Boys et al. 2008), can occur within a cycle at a deformation level that is lower than the maximum imposed deformation. This explains the choice in the present work to denote as the drift at axial failure the maximum drift and not the actual drift at which axial failure occurs.

Fig. 16 and **Table 5** summarize graphically and numerically, respectively, the values of the drift limits obtained in all the tests. In general, it can be noted that both θ_u and θ_a decrease from UM to UCA, UCS, BE and BC, and that both drift limits (particularly θ_a) tend to be lower in the VL than in the L case. Furthermore, θ_a is closer to θ_u in the tests with the higher axial load level. In these latter tests all columns fail in shear, and the observed decrease in the drift limits from UCS to UCA is explained by the fact that symmetric loading causes premature buckling and consequent loss of contribution to shear resistance given by dowel action and concrete in compression. The effect of biaxial loading can be evaluated by comparing the results of the uniaxial symmetric tests with those of the biaxial tests. It can be observed that for the lower axial load level, columns fail in flexure and biaxial loading reduces θ_u by precipitating bar buckling and consequent strength degradation. For the higher axial load level, columns fail in shear. The decrease in observed drift limits for biaxial loading is determined by the accelerated deterioration of the contribution of aggregate interlock and compressed concrete to shear resistance. In this case, spacing of the stirrups has little influence. This is probably because the accelerated concrete crushing produced by biaxial loading, rather than the bars buckling (affected by the amount of transversal reinforcement), is the main cause of reduction in the shear resistance. **Fig. 16** also reports, in red dashed-lines, the mean value of the drift ratio at ultimate as calculated according to Eurocode 8 Part 3. This is obtained through equation A.1 of CEN (2005) by assuming the partial factor γ_{el} being equal to 1. It is interesting to observe that Eurocode 8 predicts with good approximation the results of the uniaxial tests, while largely overestimates the deformation capacity of the members under biaxial loading. This quick comparison sheds some light on the need, in general, to validate with respect to observations also from multi-axial tests the models proposed by seismic codes and literature for the deformation capacity of reinforce concrete columns.

Conclusions

The tests performed confirm that the response under biaxial load paths is qualitatively and quantitatively different from that in uniaxial load paths. The first and foremost qualitative difference is that the damage mechanisms change and the failure mode can change as a result. Biaxial loading accelerates concrete crush caused by flexure, leading to a possible loss of the vertical load-bearing capacity of the column and to a switch in the failure mode from shear to flexure. In the case of flexure-shear critical columns, it produces diffused cracks and shear failure which may not exhibit a clear sliding along a dominant diagonal crack. In general, biaxial loading significantly reduces both the ultimate and the collapse deformation capacity, to values which in the case of the tested members reached approximately 60% of those measured through the uniaxial tests.

It is important to observe that this difference in response to load-path may lead to different conclusions about the effectiveness of some reinforcement details. For instance, as shown in Umemura and Ichinose (2004), the same amount of transverse reinforcement arranged in lower diameter stirrups with cross ties or in larger diameter stirrups only seem to have no effect in uniaxial bending, while they are shown to be preferable in biaxial (i.e. realistic) deformations. The tests presented in this paper also suggest that the spacing of reinforcement plays an important role in determining the performance of columns under bi-axial loading, and suggest that same transverse reinforcement ratio, if achieved with a smaller stirrup spacing, can result in a better response. This is in line with the general trend that more numerous smaller bars are preferred over fewer larger bars to control cracking.

The above findings can only be extended to members characterized by geometry, materials, and applied levels of axial load similar to those of the tested specimens, and thus not to columns which may experience large axial load variation. The effect of cyclic axial loading can indeed be significant, especially if excursions in the tensile region occur, as shown by Li et al. (1988). In this case, variability with the load path of the failure mode is likely to increase while the energy and deformation capacity of the column is expected to reduce.

In future experimental research, realism of load paths should be sought. Fast biaxial and triaxial testing should be used to aid the development and validation of more realistic response models. Furthermore, as refined nonlinear response models are of strong interest for the assessment of existing structures, reinforcement details and material properties of non-conforming members should be targeted. In particular, multi-axial response of members with smooth bars should be investigated.

Data Availability

All data generated in this experimental campaign are available at the repository of the Faculty of Engineering of the University of Porto [DOI 10.13140/RG.2.2.17191.57762]

Acknowledgments

This paper reports research developed under financial support provided by "FCT - Fundação para a Ciência e Tecnologia", Portugal, co-funded by the European Social Fund, namely through the post-doc fellowship of José Melo, with reference SFRH/BPD/115352/2016 and by Base Funding - UIDB/04708/2020 and Programmatic Funding - UIDP/04708/2020 of the CONSTRUCT - Instituto de I&D em Estruturas e Construções - funded by national funds through the FCT/MCTES (PIDDAC). Paolo Franchin and Andrea Lucchini wish to gratefully acknowledge funding for this study from University of Rome La Sapienza.

References

Berry, M., M. Parrish, and M. Eberhard. 2004. "PEER Structural Performance Database." *User's Manual, Pacific Earthquake Engineering Research Center*.

Biskinis, D., Michael Fardis, and Roupakias. 2004. "Degradation of Shear Strength of Reinforced Concrete." *ACI Structural Journal*.

Biskinis, D., Fardis, M. 2010 "Deformations at flexural yielding of members with continuous or lap-spliced bars." *Structural Concrete: Journal of the fib* 11(3): 127–138.

Bousias, Stathis N., Guido Verzeletti, Michael N. Fardis, and Eugenio Gutierrez. 1995. "Load-Path Effects in Column Biaxial Bending with Axial Force." *Journal of Engineering Mechanics* 121 (5): 596–605.

Boys, Alistair. 2009. "Assessment of the Seismic Performance of Inadequately Detailed Reinforced Concrete Columns." Edited by Des Bull and Pampanin. University of Canterbury.

Boys, Alistair, K. Bull, and Stefano Pampanin. 2008. "SEISMIC PERFORMANCE OF CONCRETE COLUMNS WITH INADEQUATE TRANSVERSE REINFORCEMENT." In *Proceedings of the 2008 New Zealand Concrete Industry Conference*.

CEN (Comité Europé en de Normalisation). 2005. European Standard EN 1998-3:2005. Eurocode 8: Design of structures for earthquake resistance, Part 3: Assessment and retrofitting of buildings. Brussels:

CEN.Crowley, H., Pinho, R. 2004. “Period-height relationship for existing european reinforced concrete buildings.” *Journal of Earthquake Engineering* 8(1): 93–119.

Elkady, Ahmed, and Dimitrios G. Lignos. 2016. “Dynamic Stability of Deep and Slender Wide-Flange Steel Columns – Full Scale Experiments.” In *Proceedings of the Annual Stability Conference Structural Stability Research Council*.

Elwood, Kenneth J., and Jack P. Moehle. 2005. “Axial Capacity Model for Shear-Damaged Columns.” *ACI Structural Journal* 102 (4): 578.

Fardis, M. N., and D. E. Biskinis. 2003. “Deformation Capacity of RC Members, as Controlled by Flexure or Shear.” In *Otani Symposium*. Vol. 511530.

FEMA. 2009. *Effects of strength and stiffness degradation on seismic response, FEMA 440A*. Federal Emergency Management Agency (FEMA). Washington, DC.

Hua Jingjing, Eberhard Marc O., Lowes Laura N., and Gu Xianglin. 2019. “Modes, Mechanisms, and Likelihood of Seismic Shear Failure in Rectangular Reinforced Concrete Columns.” *Journal of Structural Engineering* 145 (10): 04019096.

Ichinose, Toshikatsu. 1995. “Splitting Bond Failure of Columns under Seismic Action.” *ACI Structural Journal*.

———. 1996. “3D Failure of RC Columns in Biaxial Shear.” In *Proceedings of the 11th World Conference on Earthquake Engineering*.

Joh, and Shibata. 1984. “Shear Failure of RC Columns Due to Biaxial Lateral Forces.” In *Proceedings of the 8th World Conference on Earthquake Engineering*.

Kowalsky, Mervyn J., and M. J. Nigel Priestley. 2000. “Improved Analytical Model for Shear Strength of Circular Reinforced Concrete Columns in Seismic Regions.” *ACI Structural Journal* 97 (3): 388–96.

Krawinkler, H. 2009. “Loading histories for cyclic tests in support of performance assessment of structural components.” In *Proc. 3rd International Conference on Advances in Experimental Seismic Engineering, Pacific Earthquake Engineering Research (PEER) Center Annual Conference*. San Francisco, California.

Krawinkler, Helmut, A. Gupta, R. Medina, and N. Luco. 2000. “Loading Histories for Seismic Performance Testing of SMRF Components and Assemblies.” *SAC Joint Venture, Report No. SAC/BD-00/10. Richmond, CA*.

Li, Kang-Ning, Hiroyuki Aoyama, and Shunsuke Otani. 1988. “Reinforced Concrete Columns under Varying Axial Load and Bi-Directional Lateral Load Reversals.” In *Proceedings of the 9th World Conference on Earthquake Engineering, Tokyo-Kyoto, Japan,* 2–9. iitk.ac.in.

Min LL. PP. (Ministero dei Lavori Pubblici). 1997. *Istruzioni per l’applicazione delle “Norme tecniche per le costruzioni in zone sismiche” di cui al Decreto Ministeriale 16 Gennaio 1996*. Circolare 10 Aprile 1997 N. 65/AA.GG (in Italian). Italy: Ministry of Public Works.

Nojavan, A., Schultz, A. E., Haselton, C., Simathathien, S., Liu, X., and S.-H. Chao. 2015. “A New Data Set for Full-Scale Reinforced Concrete Columns under Collapse-Consistent Loading Protocols.” *Earthquake Spectra* 31(2): 1211–1231.

Opabola, E. A., and Elwood, K. J. 2021. “Collapse Performance of Nominally Identical Nonductile Circular Columns Susceptible to Failure-Mode Variability.” *Journal of Structural Engineering* 147(6). https://doi.org/10.1061/(ASCE)ST.1943-541X.0003028.

Osorio, E., J. M. Bairán, and A. R. Marí. 2012. “Effects of Cyclic Biaxial Shear Loading on the Seismic Response of RC Columns.” In *Proceedings of the 15th World Conference on Earthquake Engineering*.

Panagiotakos, Telemachos B., and Michael N. Fardis. 2001. “Deformations of Reinforced Concrete Members at Yielding and Ultimate.” *Structural Journal* 98 (2): 135–48.

Park, Young-ji, and Alfredo H. -S. Ang. 1985. “Mechanistic Seismic Damage Model for Reinforced Concrete.” *Journal of Structural Engineering*. https://doi.org/10.1061/(asce)0733-9445(1985)111:4(722).

Perus, Iztok, Dionysis Biskinis, Peter Fajfar, Michael N. Fardis, Dimitrios Lignos, and Helmut Krawinkler. 2014. “The SERIES Database of RC Elements.” In *2nd ECEES*, edited by Atilla Ansal. Istanbul: Springer. https://doi.org/10.4231/D38C9R416.2.

Pham Thanh-Phuong, and Li Bing. 2014. “Splitting Failure of Reinforced Concrete Columns.” *Journal of Structural Engineering* 140 (3): 04013081.

Priestley, M. J. Nigel, Ravindra Verma, and Yan Xiao. 1994. “Seismic Shear Strength of Reinforced Concrete Columns.” *Journal of Structural Engineering* 120 (8): 2310–29.

Qiu, Fawei, Wenfeng Li, Peng Pan, and Jiaru Qian. 2002. “Experimental Tests on Reinforced Concrete Columns under Biaxial Quasi-Static Loading.” *Engineering Structures* 24 (4): 419–28.

Rodrigues, Hugo, António Arêde, André Furtado, and Patrício Rocha. 2015a. “Seismic Rehabilitation of RC Columns Under Biaxial Loading: An Experimental Characterization.” *Structures* 3 (August): 43–56.

———. 2015b. “Seismic Behavior of Strengthened RC Columns under Biaxial Loading: An Experimental Characterization.” *Construction and Building Materials* 95 (October): 393–405.

Rodrigues, Hugo, António Arêde, Humberto Varum, and Aníbal Costa. 2013. “Damage Evolution in Reinforced Concrete Columns Subjected to Biaxial Loading.” *Bulletin of Earthquake Engineering* 11 (5): 1517–40.

Rodrigues, Hugo, Antonio Arêde, Humberto Varum, and Aníbal G. Costa. 2010. “Experimental Study on the Biaxial Bending Cyclic Behaviour of RC Columns.” In *14th ECEE*. Ohrid, Macedonia.

Rodrigues, Hugo, André Furtado, and António Arêde. 2016. “Behavior of Rectangular Reinforced-Concrete Columns under Biaxial Cyclic Loading and Variable Axial Loads.” *Journal of Structural Engineering* 142 (1): 04015085.

Rodrigues, Hugo, Humberto Varum, Antonio Arêde, and Aníbal G. Costa. 2013. “Behaviour of Reinforced Concrete Column under Biaxial Cyclic Loading—State of the Art.” *International Journal of Advanced Structural Engineering*. https://doi.org/10.1186/2008-6695-5-4.

Saatcioglu, M., and G. Ozcebe. 1989. “Response of Reinforced Concrete Columns to Simulated Seismic Loading.” *ACI Structural Journal*. https://www.concrete.org/publications/internationalconcreteabstractsportal/m/details/id/2607.

Sezen, H. 2002. “Seismic response and modeling of reinforced concrete building columns.” Ph.D. thesis in Engineering - Civil and Environmental Engineering, University of California, Berkeley.

Sezen, Halil, and Jack P. Moehle. 2004. “Shear Strength Model for Lightly Reinforced Concrete Columns.” *Journal of Structural Engineering* 130 (11): 1692–1703.

Suzuki, Y., and D. G. Lignos. (2020). “Development of collapse-consistent loading protocols for experimental testing of steel columns.” *Earthquake Engineering & Structural Dynamics* 49(2): 114–131.

Takizawa, H., and H. Aoyama. 1976. “Biaxial Effects in Modelling Earthquake Response of R/C Structures.” *Earthquake Engineering and Structural Dynamics*. https://onlinelibrary.wiley.com/doi/abs/10.1002/eqe.4290040602.

Umemura, H., and T. Ichinose. 2004. “Experimental Study on the Effects of Loading History on the Ductility Capacity of Reinforced Concrete Members.” In . iitk.ac.in. http://www.iitk.ac.in/nicee/wcee/article/13_1301.pdf.

Wang, D., Li, H.-N., Li, G. (2013). “Experimental tests on reinforced concrete columns undermulti-dimensional dynamic loadings.” *Construction and Building Materials* 47: 1167–1181.

Zhu L., Elwood K. J., and Haukaas T. 2007. “Classification and Seismic Safety Evaluation of Existing Reinforced Concrete Columns.” *Journal of Structural Engineering* 133 (9): 1316–30.

Figures

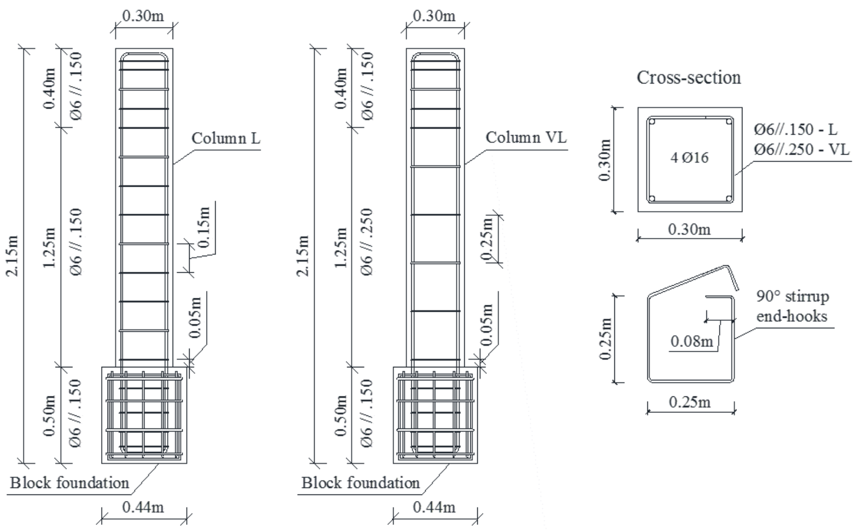

Fig. 1. Specimen geometry and reinforcement details.

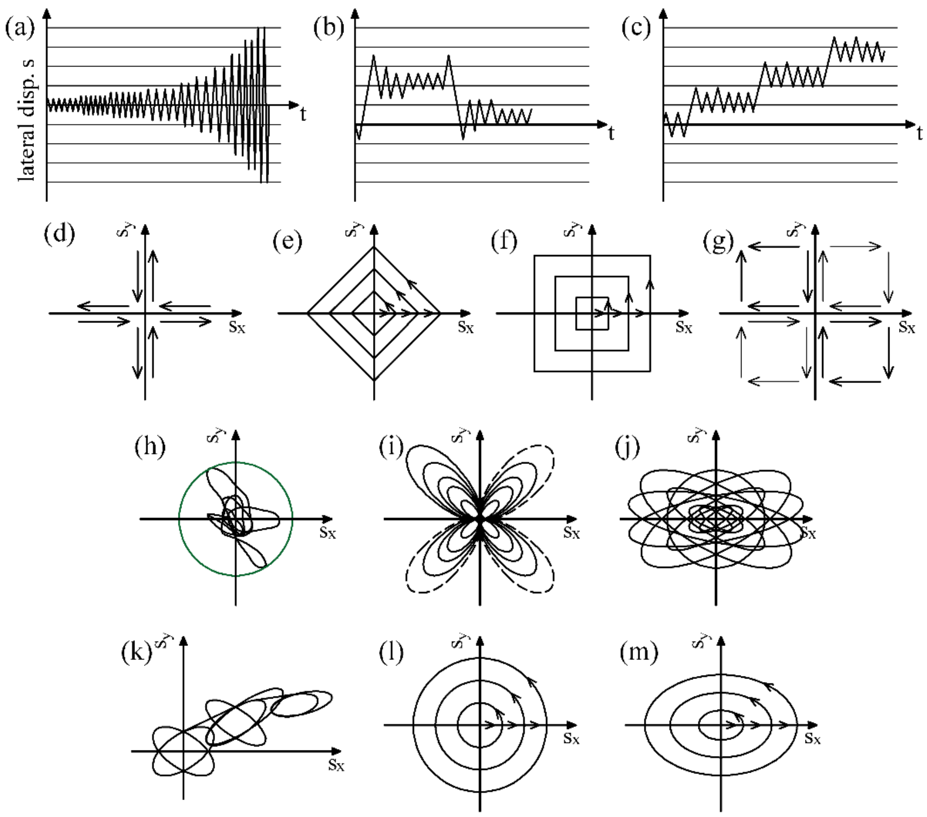

Fig. 2. Examples of uniaxial and biaxial displacement protocols used in past experimental studies.

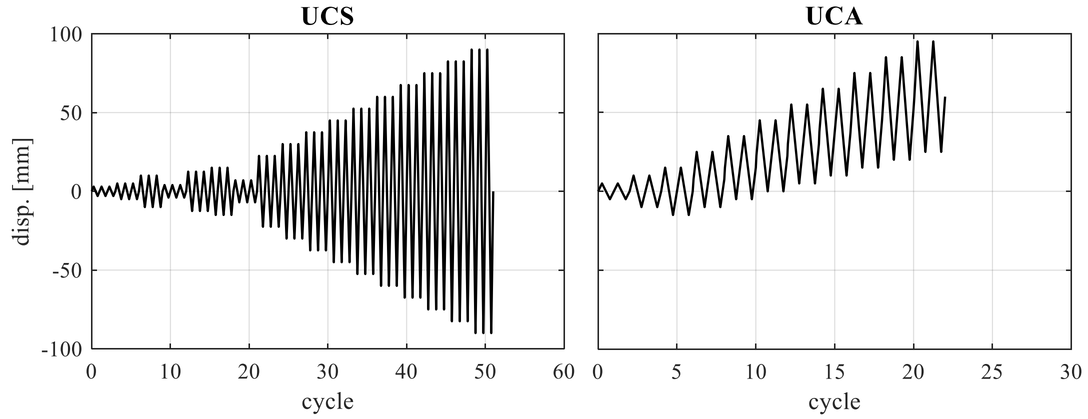

Fig. 3. Lateral displacement imposed in the uniaxial tests:

cyclic history of the symmetric (left) and the asymmetric (right) protocol.

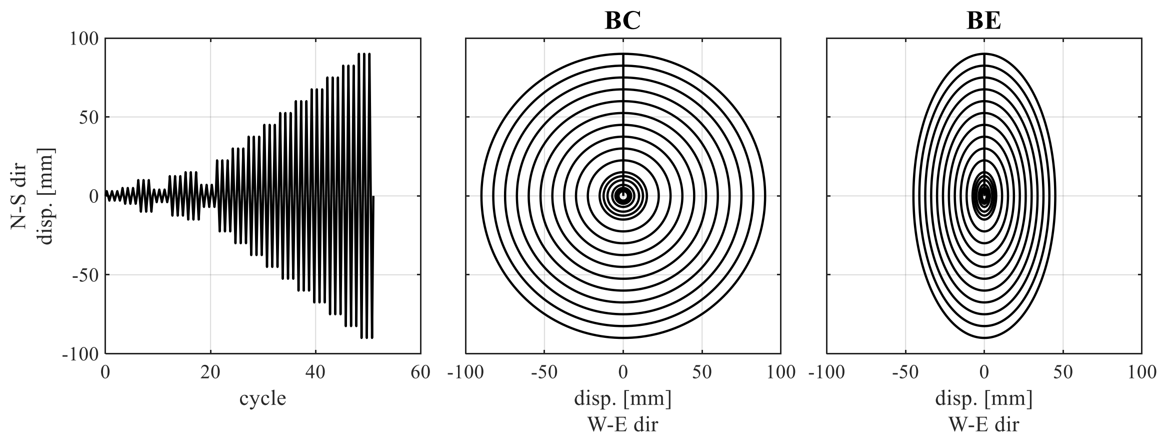

Fig. 4. Lateral displacement imposed in the biaxial tests:

cyclic history (left), and in-plan view of the circular (center) and the elliptical (right) path.

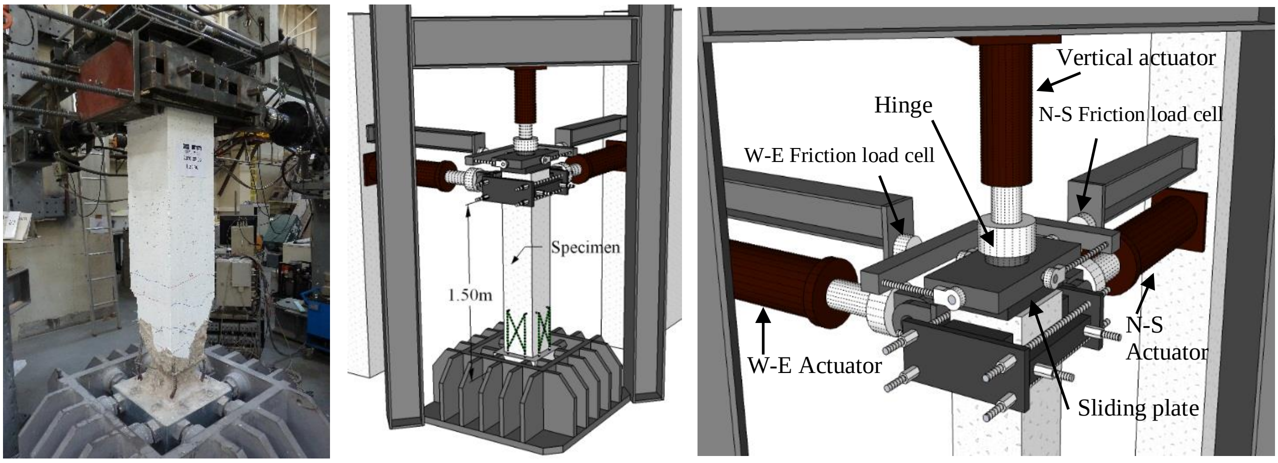

a) b) c)

Fig. 5. Experimental setup: a) general view, b) test setup schematics, c) sliding device.

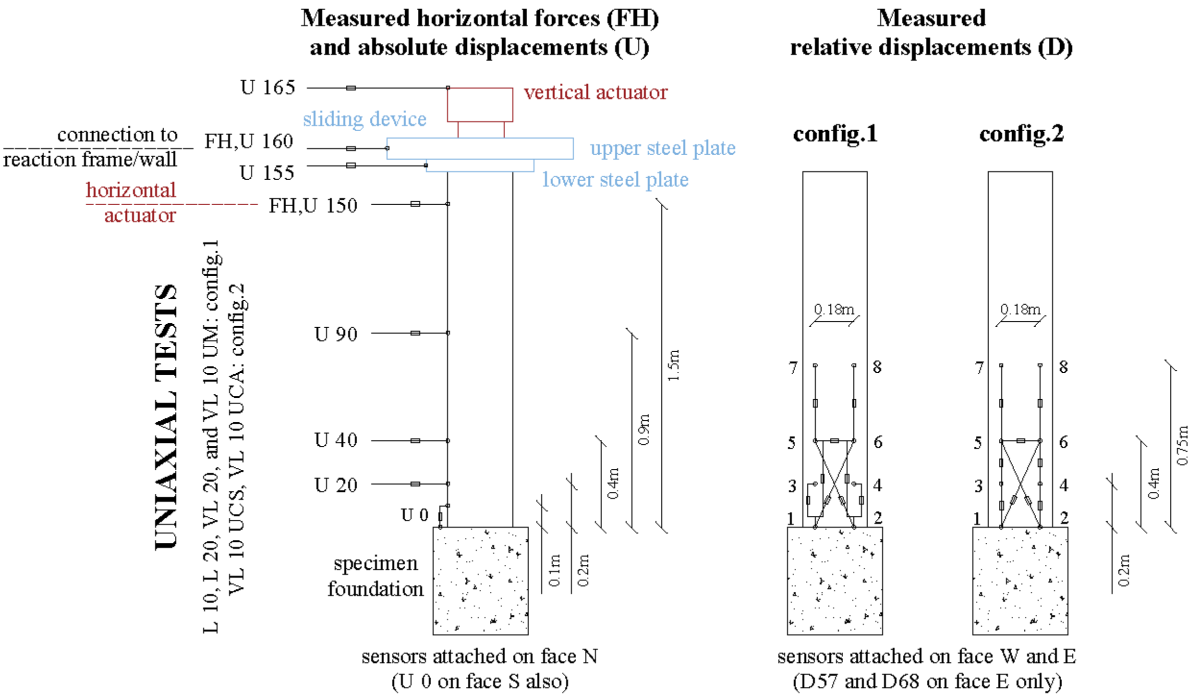

Fig. 6. Sensors used in the uniaxial tests for horizontal forces, absolute and relative displacements: labeling and location.

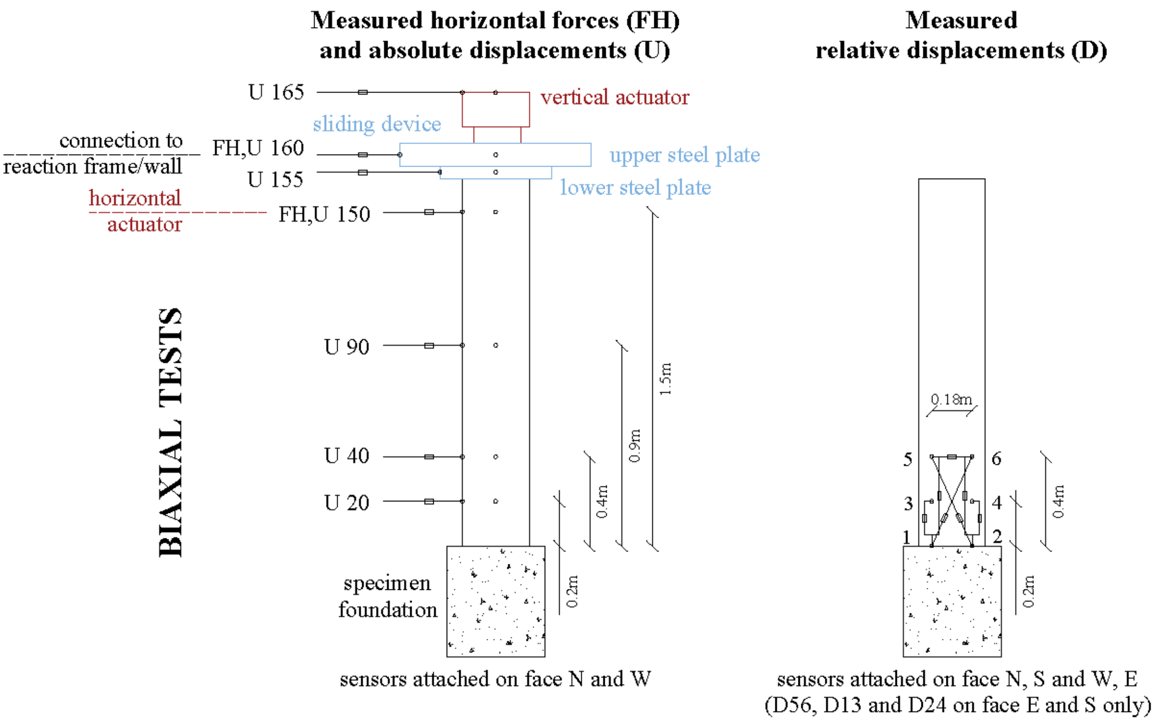

Fig. 7. Sensors used in the biaxial tests for horizontal forces, absolute and relative displacements: labeling and location.

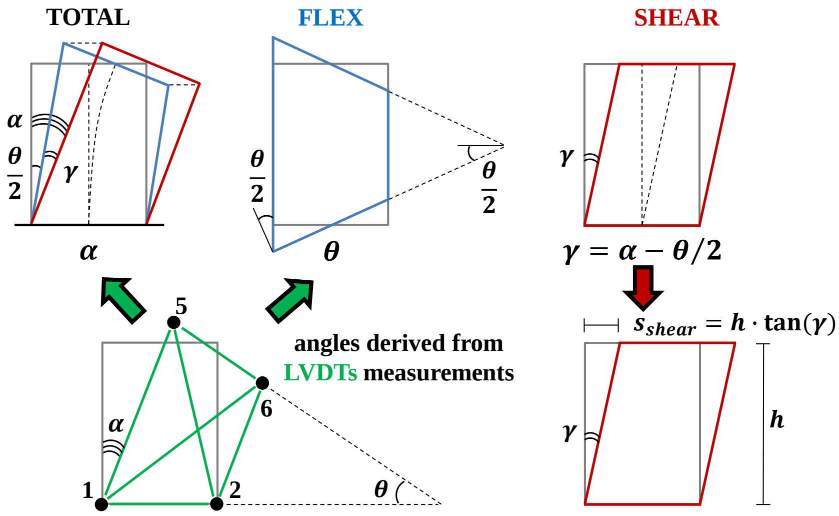

Fig. 8. Contribution of shear to lateral displacement calculated at the plastic hinge level from LVDTs measurements.

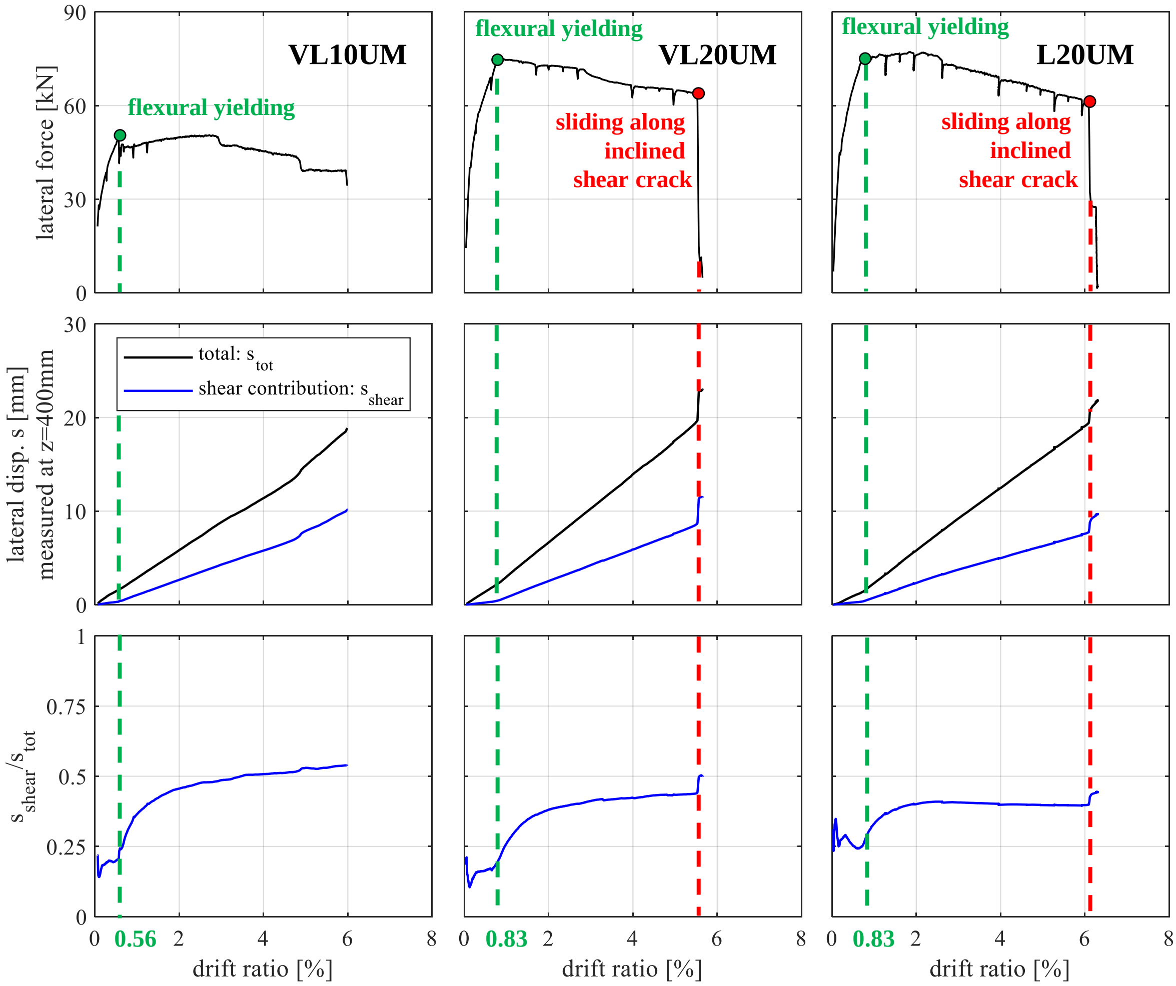

Fig. 9. Lateral force (1st row panels), and total vs calculated shear contribution of lateral displacement of point at 400 mm from the base (2nd and 3rd row plots) for the three monotonic tests.

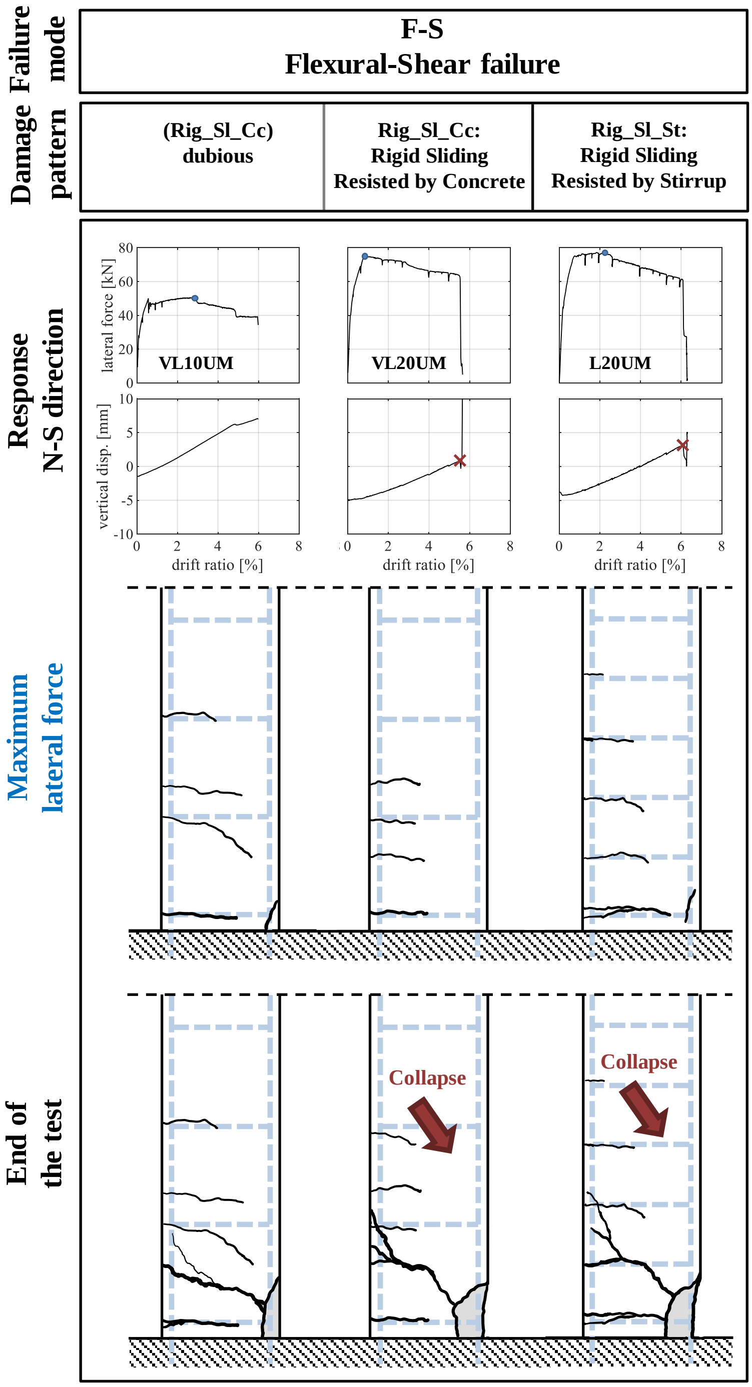

Fig. 10. Damage evolution observed in the monotonic tests.

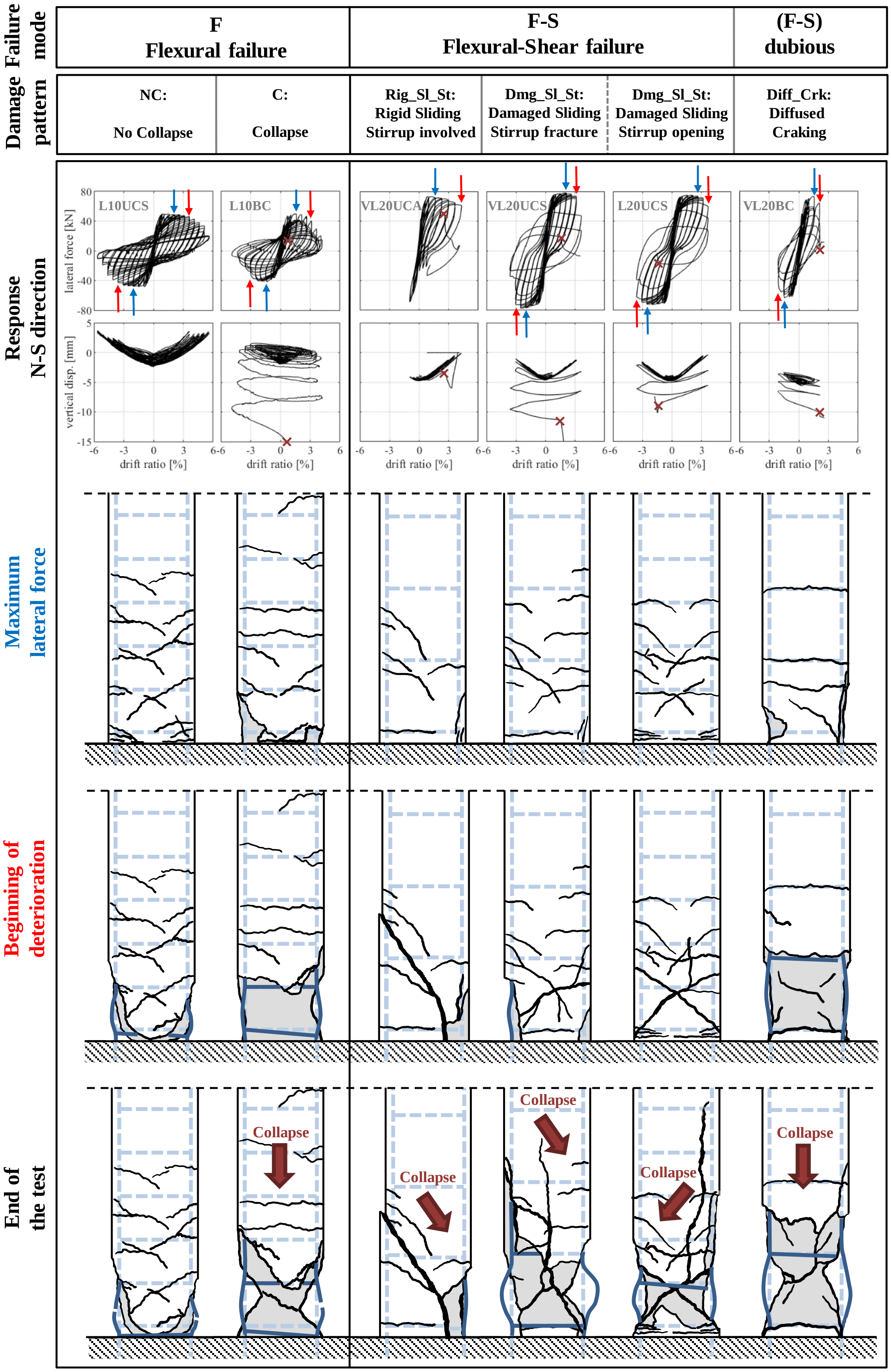
Failure mode
Damage pattern
F
Flexural failure
F-S
Flexural-Shear failure
(F-S)
dubious
NC:
No Collapse
C:
Collapse
Rig_Sl_St:
Rigid Sliding
Stirrup involved
Dmg_Sl_St:
Damaged Sliding
Stirrup fracture
Dmg_Sl_St:
Damaged Sliding
Stirrup opening
Diff_Crk:
Diffused
Craking
Response
N-S direction
L10UCS
L10BC
VL20UCA
VL20UCS
L20UCS
VL20BC
lateral force [kN]
vertical disp. [mm]
drift ratio [%]
Maximum
lateral force
Beginning of
deterioration
End of
the test
Collapse

Fig. 11. Damage evolution in columns selected to represent the six different damage patterns observed in the cyclic tests.

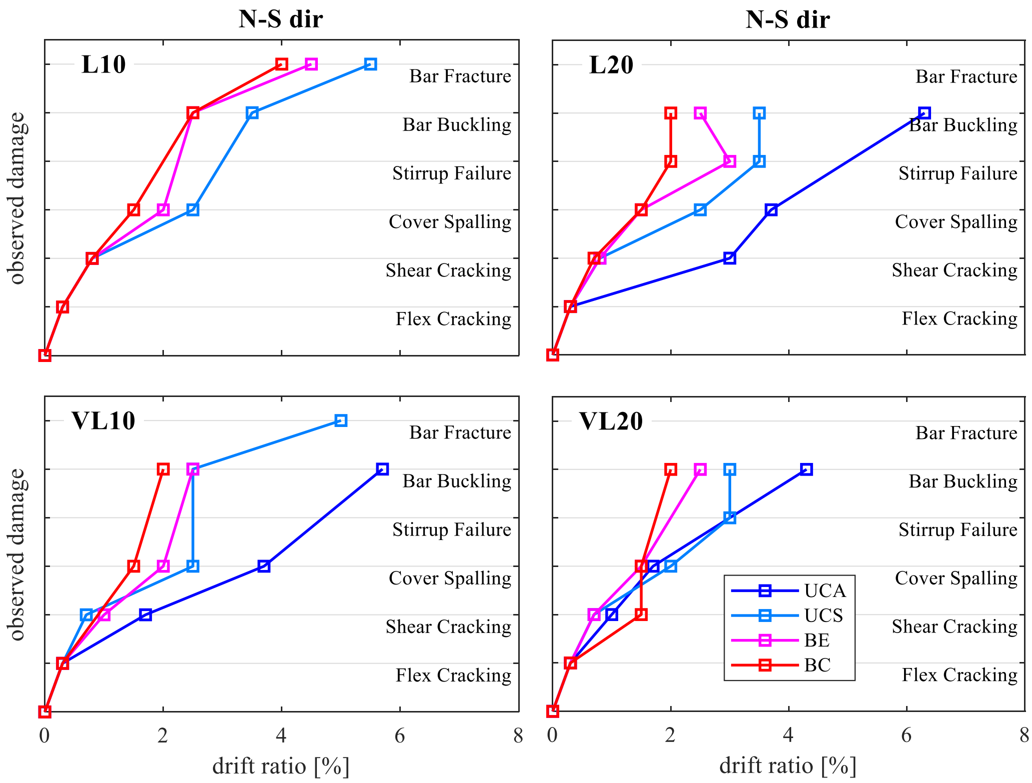

Fig. 12. Values of the drift at damage states observed in the cyclic tests.

642

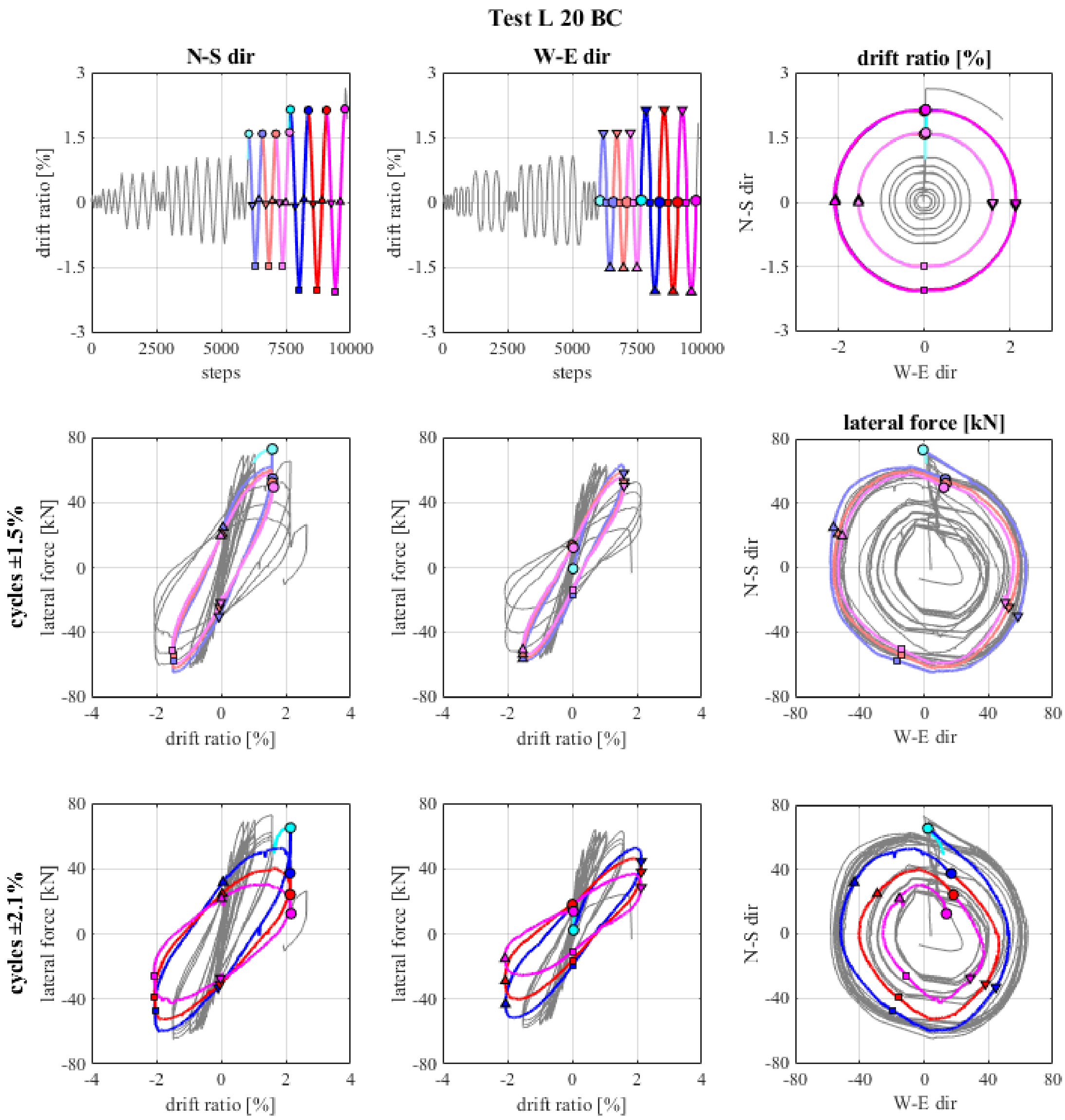

643 **Fig. 13**. Results of test L20BC selected as representative of the column's cyclic response to biaxial loading:

644 imposed drift histories (1st row panels) and measured forces (2nd and 3rd) in the two horizontal directions,

645 with highlighted two sets of cycles at a constant amplitude level equal to 1.5% and 2.1%, respectively.

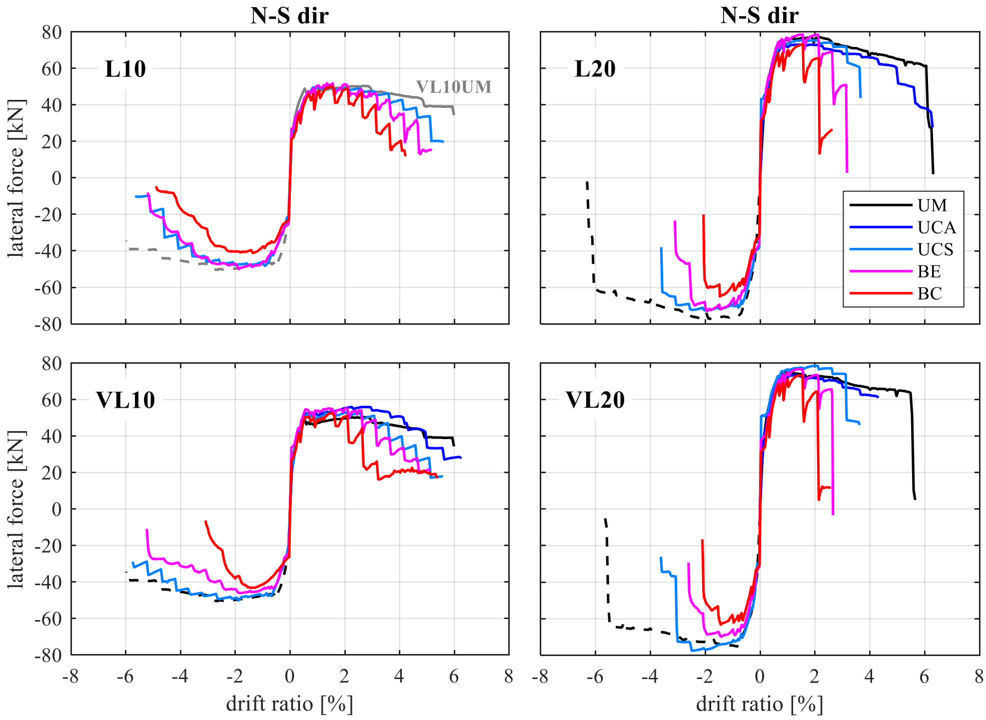

Fig. 14. Force-drift curves of the tests in the N-S direction: monotonic response (with negative branch derived as zero-point reflection of the positive one) and envelope of the cyclic response.

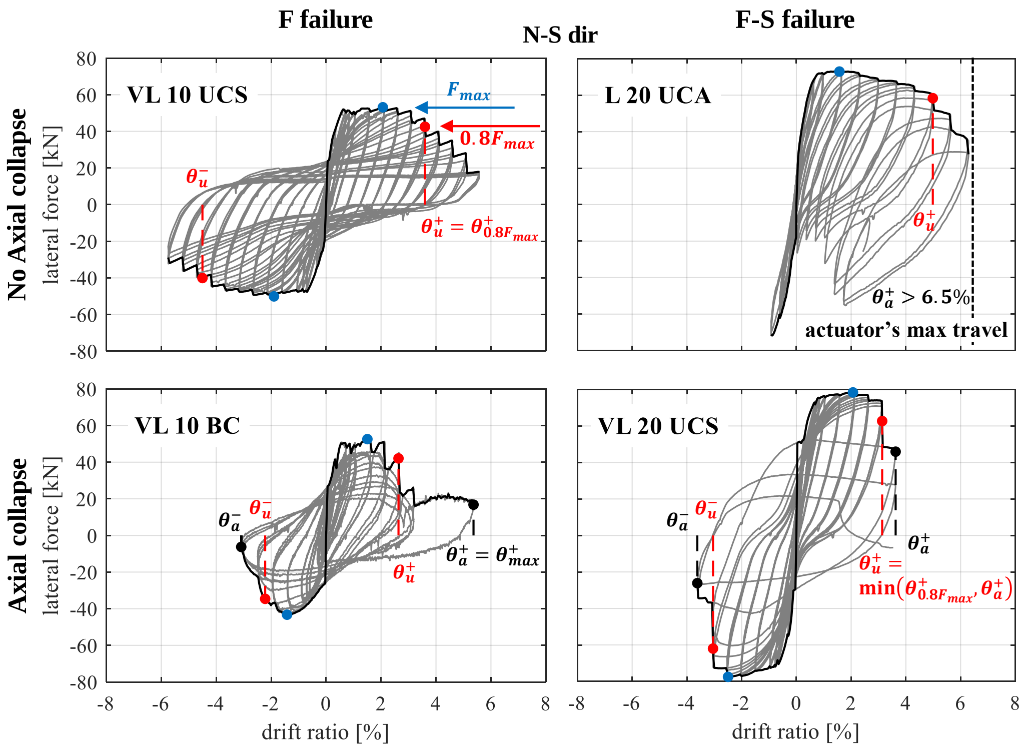

Fig. 15. Drift limits as defined for the F and F-S critical columns (left and right panels, respectively), and for the columns that exhibited loss of lateral or lateral-axial load-carrying capacity (1st and 2nd row panels, respectively).

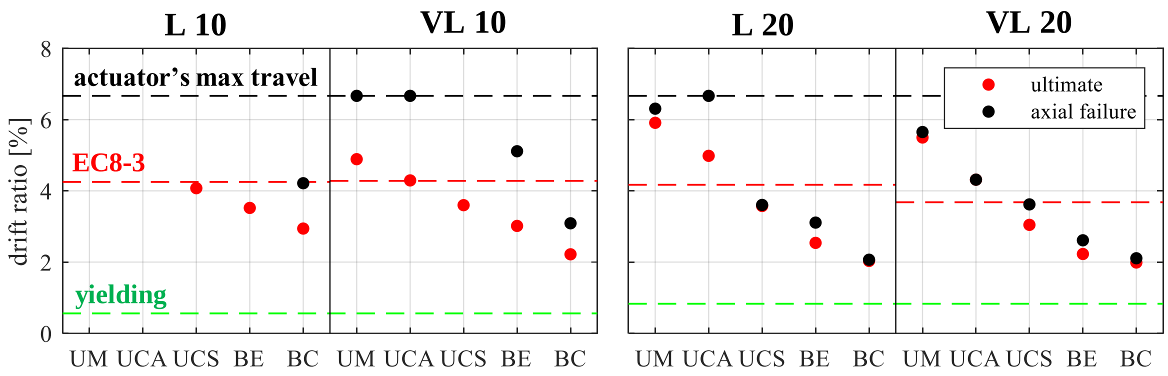

Fig. 16. Drift ratio limits as observed from tests, and drift ratio at ultimate predicted with Eurocode 8 Part 3.

Tables

Table 1. Previous experimental studies on non-uniaxial response of reinforced concrete columns

1st Author	Year	#Test Section	Loading protocol[a]	Load rate	ν	L_V/h	ρ_s [%]	Lap-splice	ρ_{sw} [%]	Failure
Joh	1984	9S 4R	13UO	S	0.0 ÷ 0.3 0.0 ÷ 0.16	1.125 ÷ 2.0	2.25	No	0.30 0.30 ÷ 0.35	S
Li	1988	7S	1U+1B+5T (g)	S	-0.06 ÷ 0.52	2.85	1.42	No	0.63	ND
Bousias	1995	12S	10B (d,f) 2T (l)	S	0.1 ÷ 0.17 0.135 ± 0.135	5.96	2.56	No[b]	0.98	F
Ichinose	1996	4S	2U+2UO	S	0.0	1.6	4.1	No	0.57 ÷ 1.01	S
Qiu	2002	7S	1U+1UO+5B (d,e,f,l)	S	0.21 ÷ 0.23	3.5	2.26	No	0.97	ND
Umemura	2004	14S	4M+3U+7B	S	0.0 ÷ 0.12	1.68	2.56	No	0.25	F-S/S
Boys	2008	6S	2U+4B (h,i)	S	0.15 ÷ 0.3	3.6	1.0	Yes	0.12	S
Rodrigues	2010	12R 4S	6U+6B (d,e,f) 1U+3B (e,f,l)	S	0.04 ÷ 0.12 0.10	3 ÷ 7.5 5	0.8 ÷ 0.94 1.0	No	0.09 ÷ 0.25 0.13	F
Osorio	2012	2C	2B (i)	S	0.20	3.64	2.49	No	0.50[c]	F-S
Wang	2013	12S	1U+4B+1T (d)	S D	0.095 ÷ 0.17	2.8 ÷ 4.3	2.26	No	0.66	F
Nojavan	2015	1R	1B	S	0.154	2.6 ÷ 3.4	1.58	No	0.89 ÷ 1.03	F
Rodrigues	2015a	6R[d]	3M+3UO	S	0.085 ÷ 0.17	3 ÷ 5	1.0	No	0.11 ÷ 0.13	F/S
Rodrigues	2015b	2R[e]	2B (e)	S	0.13	3 ÷ 5	1.0	No	0.11 ÷ 0.13	F
Rodrigues	2016	6R	6T (e,f,l)	S	0.036 ± 0.036	3 ÷ 5	1.0	No	0.11 ÷ 0.13	F

Note: cross-section is square (S), rectangular (R) or circular (C); loading is monotonic (M), uniaxial (U), uniaxial oblique (UO), biaxial (B) or triaxial (T); load rate is static (S) or dynamic (D) (50mm/s); failure mode is flexural (F), ductile-shear failure (F-S) or brittle-shear (S).

[a]Loading protocols, reported only for multi-axial cases, are indicated according to **Fig. 2** (more protocols than those in **Fig. 2** may have been used in each study, but these are not reported here).

[b]Some data are obtained from (Gutierrez, Magonette, and Verzeletti 1993).

[c]Volumetric transverse reinforcement ratio, i.e., volume of hoop to volume of core, out to out of hoop.

[d]The number of tests is ten, since four of the six specimens are retrofitted and re-tested.

[e]Seven columns of this campaign are not included because strengthened with CFRP or steel plates jacketing.

Table 2. Properties of the tested specimens

Specimen	ρ_{sw} [%]	N [kN]	f_c [MPa]	f_y [MPa]	f_u [MPa]	f_{yw} [MPa]	f_{uw} [MPa]
L10	0.126	150	21.1	433.6	584.6	459.7	565.5
VL10	0.075	150	22.4	433.6	584.6	459.7	565.5
L20	0.126	450	31.0	464.7	585.7	459.7	565.5

VL20	0.075	450	23.7	464.7	585.7	459.7	565.5

Table 3. Load paths adopted to test the specimens

	Load path				
Specimen	**UM**	**UCA**	**UCS**	**BE**	**BC**
L10	-	-	x	x	x
VL10	x	x	x	x	x
L20	x	x	x	x	x
VL20	x	x	x	x	x

Note: for each group of columns the adopted load paths are identified by the letter x.

Table 4. Failure modes and damage patterns observed in the tests

	Load path				
Specimen	**UM**	**UCA**	**UCS**	**BE**	**BC**
L10	-	-	F/NC	F/NC	F/C
VL10	(F-S/Rig_Sl_Cc)[a]	F-S/Rig_Sl_St[a]	F/NC	F/C	F/C
L20	F-S/Rig_Sl_St	F-S/Rig_Sl_St[a]	F-S/Dmg_Sl_St	(F-S)/Diff_Crk	F-S/Dmg_Sl_St
VL20	F-S/Rig_Sl_Cc	F-S/Rig_Sl_St	F-S/Dmg_Sl_St	(F-S)/Diff_Crk	(F-S)/Diff_Crk

Note: failure modes and/or damage patterns not clearly observed in the tests are reported in brackets.

[a]Tests stopped at the actuator's max travel.

Table 5. Values (in percentage) of the drift ratio from all tests at ultimate damage state and collapse (axial failure)

	Load path				
Specimen	**UM**	**UCA**	**UCS**	**BE**	**BC**
L10	-	-	4.1 ,	3.5 ,	2.9 , 4.2
VL10	4.9 , >6.5[a]	4.3 , >6.5[a]	3.6 ,	3.0 , 5.1	2.2 , 3.1
L20	5.9 , 6.3	5.0 , >6.5[a]	3.6 , 3.6	2.5 , 3.1	2.0 , 2.1
VL20	5.5 , 5.7	4.3 , 4.3	3.0 , 3.6	2.2 , 2.6	2.0 , 2.1

[a]Tests stopped at the actuator's max travel.

Appendix 1. Lateral displacement histories imposed in the cyclic tests

Fig. 3 and **Fig. 4** report the quasi-static histories of the lateral displacements imposed in the uniaxial and the biaxial cyclic tests, respectively. Note that except for few cases (i.e., VL10 UM and UCA, L20 UCA), the full displacement history was not applied because of the premature collapse of the specimen.

Appendix 2. Sequence of damage observed in the cyclic tests

Reported below a detailed description of the evolution of damage observed in the tests selected as representative of groups of columns that showed a similar failure mode, used in the text to illustrate the different damage patterns of the cyclic tests. Each damage state is associated to the amplitude of the drift in the N-S direction of the cycle the reported damage was observed at.

- L10UCS:
    - 0.3%: formation of the first flexural cracks
    - 0.8%: beginning of inclination of some cracks
    - 2.0%: inclined cracks at the base of the column at corners on face E
    - 2.5%: spalling of the concrete cover
    - 3.0%: slight widening of the inclined cracks at the base
    - 3.3%: buckling of longitudinal bars on both faces N and S
    - 4.0%: beginning of opening of the first stirrup
    - 5.3%: fracture of three longitudinal bars
- L10BC:
    - 0.3%: formation of the first flexural cracks
    - 0.8%: beginning of inclination of some cracks
    - 1.6%: spalling of the concrete cover
    - 3.0%: bar buckling and beginning of opening of the first stirrup
    - 3.3%: core crushing
    - 4.0%: fracture of one longitudinal bar
- VL20UCA:
    - 0.3%: formation of the first flexural cracks
    - 1.0%: formation of clear inclined cracks
    - 1.7%: beginning of concrete cover spalling
    - 3.0%: other inclined cracks and concrete cover crushing keep going
    - 4.3%: complete spalling of the cover, clear widening of a main inclined crack, sliding and concrete splitting at the compressed bars on face N
- VL20UCS:

- 0.3%: formation of the first flexural cracks
- 0.7%: formation of clear inclined cracks
- 1.7%: other inclined cracks
- 2.0%: spalling of the concrete cover
- 3.0%: widening of the main inclined crack at the base of the member, buckling of all bars (those on face S first), then fracture of the second stirrup, and formation of deep and large vertical cracks both along the bars on face S and at the center of the member

- L20UCS:
  - 0.3%: formation of the first flexural cracks
  - 1.2%: formation of clear inclined cracks
  - 1.0%: some vertical cracks on face S
  - 1.7%: other clear inclined cracks
  - 2.7%: beginning of concrete cover spalling
  - 3.7%: clear inclined crack through the member in both push and pull direction, core crushing, buckling of all bars, large vertical cracks along the bars on face N, opening of the second stirrup
- VL20BC:
  - 0.3%: formation of the first flexural cracks
  - 1.7%: vertical cracks and concrete spalling at the corners
  - 2.0%: large vertical cracks along the bars, core crushing and buckling of the bars, beginning of opening of the second stirrup (sequence of damage not clear)